Chaos and a quantum-classical correspondence in the kicked top

Ronald F. Fox and T. C. Elston
School of Physics, Georgia Institute of Technology, Atlanta, Georgia 30332-0430
(Received 3 June 1994)

The problem "what is the quantum signature of a classically chaotic system" is studied for the periodically kicked top. We find that the quantum variances initially grow exponentially if the corresponding classical description is chaotic. The rate of growth is connected to the corresponding classical Jacobi matrix and, thereby, to the local, classical, transient expansion rate. These connections were recently established in an analysis of the kicked pendulum for the correspondence between quantum Husimi-O'Connell-Wigner distributions and classical Gaussian ensembles. Here, we present closely related results for the kicked top by using generalized coherent states. An explanation is given for why this quantum signature of classical chaos was missed in earlier studies of the kicked top.

PACS number(s): 05.45.+b, 03.65.Bz

I. INTRODUCTION

The problems presented by the concept of quantum chaos are multifaceted [1–3]. Does it exist? If so, what is it? What are the quantum manifestations of classical chaos? How does a quantum treatment deal with classical phase space and with classical Lyapunov exponents? These questions were addressed recently for the periodically kicked pendulum [4] and for the cat map [5]. A general perspective has emerged from these studies which is elucidated in this paper with analysis of the periodically kicked top.

In the pendulum case, a smoothed Wigner distribution [6,7], the Husimi-O'Connell-Wigner distribution [8], answers the question regarding phase space, and appropriately constructed classical Gaussian ensembles manifest a quantitatively close correspondence [4]. Both the quantum variances and the classical variances initially grow exponentially if the initial distributions are sufficiently sharply peaked and the classical dynamics is chaotic [4]. The rate of growth is the same for both until saturation of the available, bounded phase space is reached. Near and after saturation, quantum interferences are seen in the evolving quantum variances but are absent from the corresponding evolving classical variances.

The exponential rate of growth of the variances depends on where in phase space the evolving distributions are initiated. The local, transient rate of expansion determines the variance growth rate for both the classical and quantum treatments [4]. For the pendulum case, this local rate of expansion, which is determined by the time evolving Jacobi matrix, is not a uniform property of the dynamics, but for the Arnold cat map it is [5]. Consequently, for the cat map, *a quantum measurement of the variance growth rate determines the largest classical Lyapunov exponent* with great accuracy.

These studies have made clear that quantum-classical correspondence exists between quantum wave packets and classical ensembles. Classical chaos creates exponential growth of the variances for both [9]. Even in the purely classical setting, the correspondence between the behavior of individual trajectories and the statistical properties of the entire ensemble breaks down rapidly for chaotic dynamics. Nevertheless, the ensemble correspondence with the quantum wave packet persists well beyond this breakdown. Two reasons contribute to failure to make these observations in numerical studies The first involves using too large a value for Planck's constant [10], or the equivalent of this, so that the initial distributions are not sufficiently sharply peaked. The second involves not constructing the correct classical ensemble correspondent for a particular quantum wave packet [11]. In our numerical studies, we have avoided the first reason by picking a sufficiently small value for Planck's constant, or an equivalent to this, and we have learned how to use appropriately smoothed wave packets in order to obtain nicely behaved classical ensemble correspondents.

In Sec. II of this paper, we present the dynamical description of the periodically kicked top. We discuss the important results from the SU(2) algebra [12] and show how to derive the corresponding classical dynamics. Generalized coherent states [2,10–12] are used to create the wave packets, and they are used a second time in order to introduce the smoothing. The construction of the appropriate classical ensemble correspondents is explained. In Sec. III, we present our numerical results. The details of our computational procedure are given and comparisons with earlier work [2,10,11] is emphasized. In Sec. IV, concluding remarks are made.

II. THE KICKED TOP

The kicked top is described by the Hamiltonian [11]

$$H = pJ_y + k\frac{J_z^2}{2j}\sum_{n=-\infty}^{\infty}\delta(t-n)\ , \tag{1}$$

in which Planck's constant $\hbar$ has been set equal to 1, p and k are parameters, and

$$[J_i, J_j] = i\varepsilon_{ijk}J_k\ , \tag{2}$$

in which ε_{ijk} is the completely antisymmetric Levi-Cività symbol. The corresponding Floquet operator for just after a kick to just after the next kick is

$$F=\exp\left[-ik\frac{J_z^2}{2j}\right]\exp[-ipJ_y]\ . \tag{3}$$

Alternatively, the Hamiltonian may be given by [10]

$$H=AS_z^2-\mu BS_x\sum_{n=-\infty}^{\infty}\delta(t-2\pi n)\ , \tag{4}$$

where

$$[S_i,S_j]=i\hbar\varepsilon_{ijk}S_k\ . \tag{5}$$

The corresponding Floquet operator for just after a kick to just after the next kick is given by

$$F=\exp\left[\frac{i}{\hbar}\mu BS_x\right]\exp\left[-\frac{i}{\hbar}2\pi AS_z^2\right]\ , \tag{6}$$

or for just before a kick to just before the next kick by

$$F=\exp\left[-\frac{i}{\hbar}2\pi AS_z^2\right]\exp\left[\frac{i}{\hbar}\mu BS_x\right]\ . \tag{7}$$

In spite of the different roles for the linear and quadratic operator terms in Eqs. (1) and (4), the Floquet operators are clearly easily interconverted. The difference between using S_x in Eq. (6) and J_y in Eq. (3) is minor since we have

$$\exp\left[-i\frac{\pi}{2}J_z\right]J_x\exp\left[i\frac{\pi}{2}J_z\right]=J_y \tag{8}$$

from Eq. (2). In the following presentation, we use the Floquet operator in Eq. (3), and discuss the work of Nakamura and co-workers [10] by the interconversion elucidated above.

The quantum map is created by the kick to kick time evolution generated by the Floquet operator F, in Eq. (3). It is natural to choose the simultaneous eigenstates of J^2 and J_z as a basis:

$$J^2|j,m\rangle=j(j+1)|j,m\rangle\ , \tag{9}$$

$$J_z|j,m\rangle=m|j,m\rangle\ . \tag{10}$$

The matrix elements of F in these states are simply

$$\langle j,m|F|j,m'\rangle=\exp\left[-i\frac{k}{2j}m^2\right]d^{(j)}_{mm'}(p) \tag{11}$$

in which the $d^{(j)}_{mm'}(p)$'s are the Wigner d functions [13].

The corresponding classical map is found [11] by interpreting the quantum description with the Heisenberg picture in which the operators evolve according to

$$\mathbf{J}(t+1)=F^{\dagger}\mathbf{J}(t)F\ . \tag{12}$$

Using Eqs. (2) and (3), we implement this evolution in two steps [11]. The first step is

$$\tilde{J}_x=\exp[ipJ_y]J_x\exp[-ipJ_y]$$
$$=J_x\cos(p)+J_z\sin(p)\ , \tag{13}$$

$$\tilde{J}_y=\exp[ipJ_y]J_y\exp[-ipJ_y]=J_y\ , \tag{14}$$

$$\tilde{J}_z=\exp[-ipJ_y]J_z\exp[-ipJ_y]$$
$$=J_z\cos(p)-J_x\sin(p)\ , \tag{15}$$

in which the $\mathbf{J}$ components on the right-hand side are for time t. In the second step, we need

$$\mathbf{J}(t+1)=\exp\left[i\frac{k}{2j}\tilde{J}_z^2\right]\tilde{\mathbf{J}}(t)\exp\left[-i\frac{k}{2j}\tilde{J}_z^2\right]\ . \tag{16}$$

These expressions are most easily reduced using the following angular momentum algebra identities:

$$\tilde{J}_z^2=\tilde{\mathbf{J}}^2-\tilde{J}_+\tilde{J}_-+\tilde{J}_z\ , \tag{17}$$

where

$$\tilde{J}_{\pm}=\tilde{J}_x\pm i\tilde{J}_y\ , \tag{18}$$

$$[\tilde{J}_z,\tilde{J}_{\pm}]=\pm\tilde{J}_{\pm}\ , \tag{19}$$

$$[\tilde{J}_+,\tilde{J}_-]=2\tilde{J}_z\ , \tag{20}$$

$$[\tilde{J}_+\tilde{J}_-,\tilde{J}_z]=0\ , \tag{21}$$

$$[\tilde{J}_+\tilde{J}_-,\tilde{J}_+]=-2\tilde{J}_+\tilde{J}_z\ , \tag{22}$$

$$[\tilde{J}_+\tilde{J}_-,\tilde{J}_-]=2\tilde{J}_z\tilde{J}_-\ . \tag{23}$$

These imply

$$J_x(t+1)=\tfrac{1}{2}\tilde{J}_+\exp\left[i\frac{k}{2j}(2\tilde{J}_z+1)\right]$$
$$+\tfrac{1}{2}\exp\left[-i\frac{k}{2j}(2\tilde{J}_z+1)\right]\tilde{J}_-\ , \tag{24}$$

$$J_y(t+1)=\frac{1}{2i}\tilde{J}_+\exp\left[i\frac{k}{2j}(2\tilde{J}_z+1)\right]$$
$$-\frac{1}{2i}\exp\left[-i\frac{k}{2j}(2\tilde{J}_z+1)\right]\tilde{J}_-\ , \tag{25}$$

$$J_z(t+1)=\tilde{J}_z\ . \tag{26}$$

The classical map emerges in the limit where noncommutivity is negligible and the Heisenberg operators are reinterpreted as classical variables [11]:

$$J_x(t+1)=\tfrac{1}{2}[J_x\cos(p)+J_z\sin(p)+iJ_y]\exp\left[i\frac{k}{2j}\{2[J_z\cos(p)-J_x\sin(p)]+1\}\right]+\text{c.c.}\ , \tag{27}$$

$$J_y(t+1)=\frac{1}{2i}[J_x\cos(p)+J_z\sin(p)+iJ_y]\exp\left[i\frac{k}{2j}\{2[J_z\cos(p)-J_x\sin(p)]+1\}\right]+\text{c.c.}\ , \tag{28}$$

$$J_z(t+1)=J_z\cos(p)-J_x\sin(p)\ . \tag{29}$$

To obtain a sharply peaked initial wave packet, we use a generalized SU(2) coherent state [12], since it will minimize the initial uncertainty product. Such a state may be defined [2,10,11] by

$$\begin{aligned}|\theta,\phi\rangle&=\exp\{i\theta[J_x\sin(\phi)-J_y\cos(\phi)]\}|j,j\rangle\\&=(1+\tau\tau^*)^{-j}\exp[\tau J_-]|j,j\rangle\\&=(1+\tau\tau^*)^{-j}\sum_{m=-j}^{j}\tau^{j-m}\left[\frac{2j!}{(j+m)!(j-m)!}\right]^{1/2}|j,m\rangle\ ,\end{aligned} \tag{30}$$

where

$$\tau=\exp[i\phi]\tan\left[\frac{\theta}{2}\right]\ . \tag{31}$$

Its properties are given succinctly by [2]

$$\langle\theta,\phi|j_z|\theta,\phi\rangle=j\cos(\theta)\ , \tag{32}$$

$$\langle\theta,\phi|J_\pm|\theta,\phi\rangle=j\exp[\pm i\phi]\sin(\theta)\ , \tag{33}$$

$$\frac{1}{j^2}(\langle\theta,\phi|\mathbf{J}^2|\theta,\phi\rangle-\langle\theta,\phi|\mathbf{J}|\theta,\phi\rangle^2)=\frac{1}{j}\ . \tag{34}$$

These identities justify the interpretation that the coherent state $|\theta,\phi\rangle$ essentially points in the direction of the Cartesian unit vector

$$\mathbf{n}=\mathbf{k}\cos(\theta)+\mathbf{i}\sin(\theta)\cos(\phi)+\mathbf{j}\sin(\theta)\sin(\phi)\ , \tag{35}$$

with a solid angle uncertainty of $\Delta\Omega=1/j$. Since $\hbar=1$ here, the classical limit amounts to $j\to\infty$, in which limit the uncertainty vanishes.

It is tempting to use $|\theta,\phi\rangle$ directly to obtain the corresponding classical ensemble. It is easy to show from Eq. (30) that

$$\begin{aligned}\Psi(\theta,\phi;\theta',\phi')=&(1+\tau\tau^*)^{-j}\\&\times\sum_{m=-j}^{j}\tau^{j-m}\left[\frac{2j!}{(j+m)!(j-m)!}\right]^{1/2}\\&\times Y_{jm}(\theta',\phi')\ ,\end{aligned} \tag{36}$$

in which the $Y_{jm}(\theta',\phi')$'s are the normalized spherical harmonics and $\Psi(\theta,\phi;\theta',\phi')$ is the Schrödinger state labeled by (θ,ϕ) with variables (θ',ϕ'). The squared modulus of this Schrödinger state is a probability distribution in (θ',ϕ') labeled by (θ,ϕ). It may be used to describe the classical ensemble. However, this probability distribution is a double m sum that does not simplify and does not lead to an easily tractable $j\to\infty$ limit.

An alternative approach is suggested by the smoothed Wigner distribution used in the treatment of the kicked pendulum [4,6]. The Husimi-O'Connell-Wigner distribution [8] is the result of Gaussian smoothing. In a fundamental paper [7], Chang and Shi have shown that smoothing of the Wigner distribution facilitates the quantum-classical transition.

Let $|\Psi\rangle$ denote an arbitrary state for a system with one degree of freedom, q. The Wigner distribution may be written [7]

$$D_W(q',p')=\frac{1}{(2\pi\hbar)^{1/2}}\int dx\,\exp\left[-\frac{i}{\hbar}p'x\right]\left\langle q'+\frac{x}{2}|\Psi\right\rangle\times\left\langle\Psi|q'-\frac{x}{2}\right\rangle\ . \tag{37}$$

As is well known, this expression is not always positive and, therefore, is not a true probability distribution. Let $|\alpha\rangle$ for complex α denote a harmonic oscillator (with mass $m=1$) coherent state. If we write $\alpha=\alpha_1+i\alpha_2$, then it follows [7,14] that

$$\begin{aligned}\langle q'|\alpha\rangle=&\left[\frac{\omega}{\pi\hbar}\right]^{1/4}\exp[-i\alpha_1\alpha_2]\\&\times\exp\left[-\left[\left[\frac{\omega}{2\hbar}\right]^{1/2}q'-\alpha_1\right]^2+2i\alpha_2\left[\frac{\omega}{2\hbar}\right]^{1/2}q'\right]\ ,\end{aligned} \tag{38}$$

$$\begin{aligned}\langle p'|\alpha\rangle=&\left[\frac{1}{\pi\hbar\omega}\right]^{1/4}\exp[i\alpha_1\alpha_2]\\&\times\exp\left[-\left[\left[\frac{1}{2\hbar\omega}\right]^{1/2}p'-\alpha_2\right]^2-2i\alpha_1\left[\frac{1}{2\hbar\omega}\right]^{1/2}p'\right]\ .\end{aligned} \tag{39}$$

Therefore, the probability distribution associated with $|\alpha\rangle$ is Gaussian in both q' and p', is centered at $[(2\hbar/\omega)^{1/2}\alpha_1,\ (2\hbar\omega)^{1/2}\alpha_2]=(q,p)$, and has variances $\hbar/2\omega$ and $\hbar\omega/2$, respectively. While the coherent states are overcomplete, they are a very useful basis and provide a resolution of the identity I given by [14]

$$\frac{1}{\pi}\int d\alpha^2|\alpha\rangle\langle\alpha|=I\ . \tag{40}$$

A Gaussian smoothing of $D_W(q',p')$ with the Gaussian parameters associated with the coherent state $|\alpha\rangle$ is given by

$$D_H(q,p)=\frac{1}{\pi}|\langle\alpha|\Psi\rangle|^2\ . \tag{41}$$

In this expression, we have divided the published expression [7] by π so that Eq. (40) may be used together with Eqs. (38) and (39) to write the normalization integral

$$\int \frac{dqdp}{h} D_H(q,p)=1 , \tag{42}$$

in which we correctly see Planck's constant h and not the usual $\hbar$. The analog of this detail regarding normalization is crucial in our generalized coherent state treatment of the kicked top which follows. D_H is a proper probability distribution and is equivalent with the Gaussian wave packets we used in our earlier kicked pendulum studies [4].

These results suggest that smoothing may be useful in the case of the kicked top as well. In this case, it seems appropriate to use the SU(2) generalized coherent states instead of harmonic oscillator coherent states. Thus we are naturally led to a generalized Husimi-O'Connell-Wigner distribution given tentatively by

$$D_H(\theta',\phi';\theta,\phi)=|\langle \theta',\phi'|\theta,\phi\rangle|^2 . \tag{43}$$

Using Eq. (30) for $|\theta,\phi\rangle$ and a similar expression for $|\theta',\phi'\rangle$, we obtain

$$\begin{aligned}\langle \theta',\phi'|\theta,\phi\rangle &= \cos^{2j}\left(\frac{\theta'}{2}\right)\cos^{2j}\left(\frac{\theta}{2}\right)\sum_{m=-j}^{j}(\tau'^{*}\tau)^{j-m}\frac{2j!}{(j+m)!(j-m)!} \\ &= \cos^{2j}\left(\frac{\theta'}{2}\right)\cos^{2j}\left(\frac{\theta}{2}\right)\sum_{n=0}^{2j}(\tau'^{*}\tau)^{2j-n}\frac{2j!}{n!(2j-n)!} \\ &= \cos^{2j}\left(\frac{\theta'}{2}\right)\cos^{2j}\left(\frac{\theta}{2}\right)\left[1+\exp[i(\phi-\phi')]\tan\left(\frac{\theta'}{2}\right)\tan\left(\frac{\theta}{2}\right)\right]^{2j} .\end{aligned} \tag{44}$$

By means of trigonometric identities, this leads to

$$D_H(\theta',\phi';\theta,\phi)=(\tfrac{1}{2}[1+\cos(\gamma)])^{2j} , \tag{45}$$

where

$$\begin{aligned}\cos(\gamma) &= \cos(\theta')\cos(\theta)+\cos(\phi-\phi')\sin(\theta')\sin(\theta) \\ &= \mathbf{n}'\cdot\mathbf{n} ,\end{aligned} \tag{46}$$

in which Eq. (35) has been invoked. There is duality regarding the interpretation of (θ',ϕ') and (θ,ϕ) as labels and variables.

Qualitatively [10], it is clear that, as $j\to\infty$,

$$(\tfrac{1}{2}[1+\cos(\gamma)])^{2j}\to\begin{cases}1 & \text{for } \gamma=0\\ 0 & \text{otherwise.}\end{cases} \tag{47}$$

The meaning of $\gamma=0$ is clear from Eq. (46); it means $\theta=\theta'$ and $\phi=\phi'$. The SU(2) generalized coherent states $|\theta,\phi\rangle$ are overcomplete and yield a resolution of the identity operator I given by [12]

$$\frac{2j+1}{4\pi}\int d\Omega'|\theta',\phi'\rangle\langle\theta',\phi'|=I , \tag{48}$$

in which (θ',ϕ') are now state labels for the smoothing states. This means that $|\langle\theta',\phi'|\theta,\phi\rangle|^2$ is not properly normalized, i.e., we must amend Eq. (43) by writing

$$D_H(\theta',\phi';\theta,\phi)=\frac{2j+1}{4\pi}|\langle\theta',\phi'|\theta,\phi\rangle|^2 , \tag{49}$$

so that

$$\int d\Omega' D_H(\theta',\phi';\theta,\phi)=1 . \tag{50}$$

Therefore, the classical distribution $P(\theta',\phi')$ is given by

$$P(\theta',\phi')=\lim_{j\to\infty}\frac{2j+1}{4\pi}(\tfrac{1}{2}[1+\cos(\gamma)])^{2j} . \tag{51}$$

Writing $(\frac{1}{2}[1+\cos(\gamma)])^{2j}$ as

$$(\tfrac{1}{2}[1+\cos(\gamma)])^{2j}=\exp\{2j(\ln[1+\cos(\gamma)]-\ln 2)\} , \tag{52}$$

and expanding the exponent around its maximum at $\theta=\theta'$ and $\phi=\phi'$ produces

$$P(\theta',\phi')=\frac{2j+1}{4\pi}\exp\left[-\frac{j}{2}(\theta-\theta')^2-\frac{j}{2}\sin^2(\theta)(\phi-\phi')^2\right] \tag{53}$$

for very large j. With the solid angle measure $d\Omega'$ it is seen that this distribution is a properly normalized Gaussian distribution in both θ' and ϕ'.

By using the precise normalized form of the classical limit distribution given in Eq. (53), we are able to obtain substantial quantitative refinements of previously published results [2,10,11]. The presence of $\sin^2(\theta)$ in the distribution enables us to examine any value of the label θ, and not just the value $\pi/2$ examined previously [10]. Moreover, the use of a genuine Gaussian distribution is found to be quantitatively superior to the uniform disk distributions [10,11] used in the earlier work. These facts are exhibited in Sec. III.

There is one additional subtlety to be noted. From Eqs. (32) and (33), it is clear that the classical variables are

$$J_x=j\sin(\theta')\cos(\phi') , \tag{54}$$

$$J_y=j\sin(\theta')\sin(\phi') , \tag{55}$$

$$J_z=j\cos(\theta') . \tag{56}$$

If we use Eq. (53) to compute the classical analog to Eq. (34), we obtain

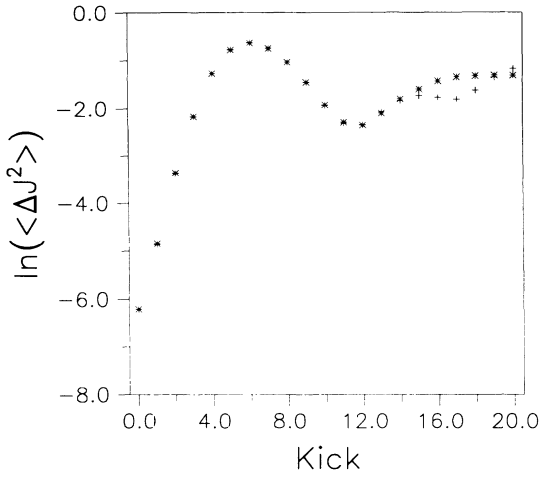

FIG. 1. Quantum and classical evolution of the variance of the total angular momentum as a function of kick number. Plus signs are for the quantum results, and asterisks are for the classical results. $p=\pi/2$, $k=2.4$, and $j=500$. $\theta=\pi/2$ and $\phi=\pi/2$. The classical ensemble contains 5000 points.

$$\frac{1}{j^2}\left[\int d\Omega' P(\theta',\phi')\mathbf{J}^2-\left[\int d\Omega' P(\theta',\phi')\mathbf{J}\right]^2\right]$$
$$=\frac{1}{j}\cos^2(\theta)+\frac{1}{j}\left[1+\frac{1}{\sin^2(\theta)}\right]\sin^2(\theta)$$
$$=\frac{2}{j}\ , \tag{57}$$

which is twice as large as in Eq. (34). This factor of 2 is caused by the generalized coherent state smoothing of a generalized coherent state, each of which contributes a variance of $1/j$, and the fact that the variances of Gaussian products add. Consequently, if we study a quantum wave packet coherent state $|\theta,\phi\rangle$ and use $P(\theta',\phi')$ for the classical ensemble distribution, we must use $2j$ in $P(\theta',\phi')$ when we use j in $|\theta,\phi\rangle$. Our numerical results, exhibited in Sec. III, clearly demonstrate the high degree of quantitative correspondence achievable when this observation is heeded.

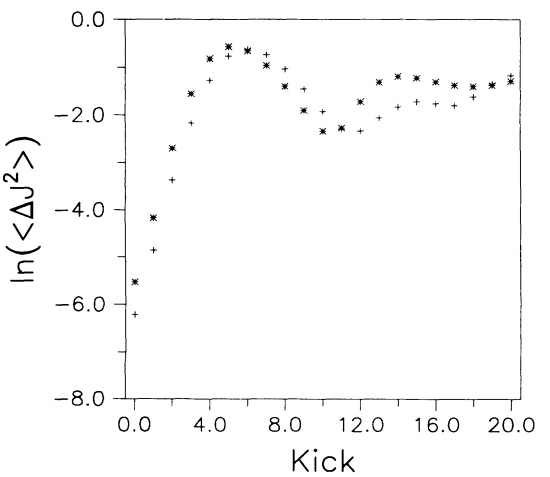

FIG. 2. The same quantities and parameters as in Fig. 1, but with a uniform circular disk for the initial classical ensemble.

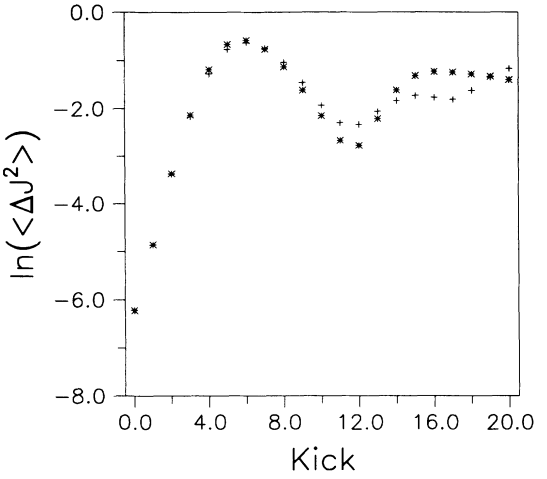

FIG. 3. The same quantities and parameters as in Fig. 2, but with a uniform circular disk satisfying Eq. (57) for the initial classical ensemble.

III. NUMERICAL RESULTS

The numerical computations exhibited below demonstrate the concepts developed in Sec. II. The quantum version is performed by evolving the generalized coherent state given in Eq. (30) with the Floquet matrix given in Eq. (11). For a specific choice of parameters θ and ϕ for the initial, generalized coherent state $|\theta,\phi\rangle$, the coefficients of the basis states $|j,m\rangle$ are determined by the last line of Eq. (30). The presence of the factorials in these coefficients and also in the Wigner d functions in the Floquet matrix require special treatment. This is achieved by using expressions giving the Wigner d func-

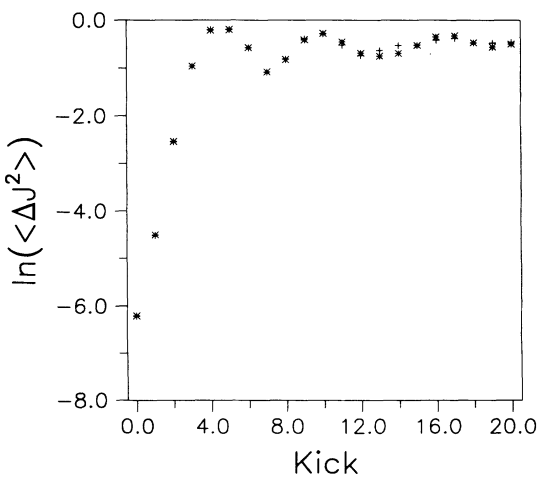

FIG. 4. The same quantities and parameters as in Fig. 1, except that $k=3.0$.

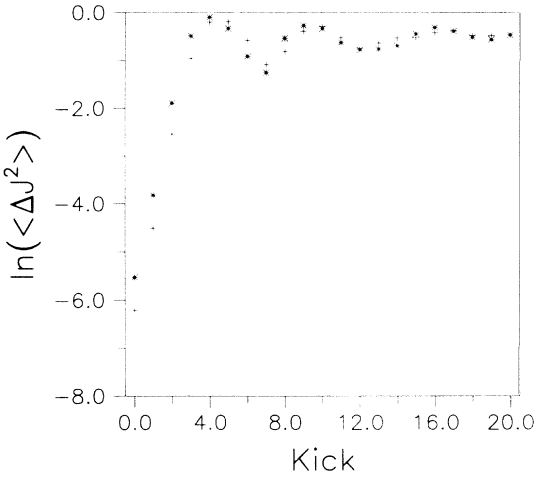

FIG. 5. The same quantities and parameters as in Fig. 2, except that $k=3.0$.

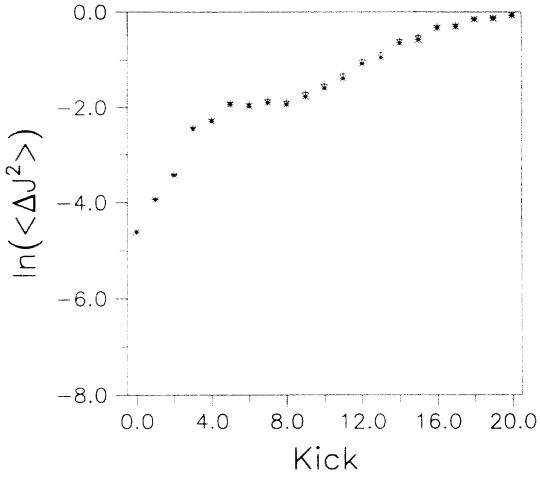

FIG. 7. The same quantities and parameters as in Fig. 1, except that $k=1.865$, $j=100$, $\theta=\pi/4$, and $\phi=\pi/4$.

tions in terms of Jacobi polynomials [15] and using well established numerical routines for the Jacobi polynomials, and Stirling's logarithmic treatment of the remaining factorials. The classical version is performed by generating an ensemble of initial points, (θ,ϕ), in accord with the classical probability distribution given in Eq. (53). Since this distribution is Gaussian in both variables, we can implement the generation of the initial ensemble using the Box-Muller algorithm [16]. However, in accord with the discussion at the end of Sec. II, when we use j for the quantum evolution, we must use $2j$ for the classical evolution. This is because we use a generalized coherent state for the quantum evolution but use a generalized coherent state smoothed by another generalized coherent state for the classical evolution.

Figure 1 shows both the quantum and classical evolutions of the natural logarithm of the variance of the total angular momentum as a function of kick for 20 kicks. The plus signs are for the quantum results and the asterisks are for the classical results. It is clear that the results are indistinguishable until kick 10 after which small differences are discerned. The parameter values $p=\pi/2$, $k=2.4$, and $j=500$ have been used in Eq. (11). The generalized coherent state angles are $\theta=\pi/2$ and $\phi=\pi/2$. The nearly linear initial growth stage of the semilog plot means that the variances grow nearly exponentially until saturation of the bounded phase space occurs around kick 6. Because both the classical and quantum results coincide, the rate of growth of the quantum variance reproduces the local expansion rate of the classical dynamics, which may be thought of as a local, transient Lyapunov exponent [4]. This is not the same as the global Lyapunov exponent that requires an ergodic sampling of the entire attractor. These observations parallel the kind of results we obtained earlier for the kicked pendulum [4]. The initial exponential growth stage seen here is

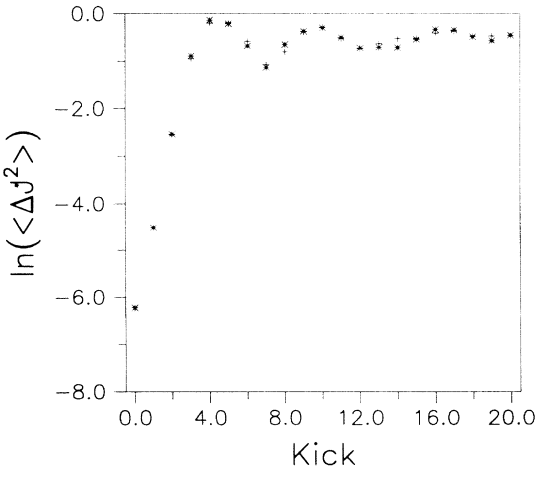

FIG. 6. The same quantities and parameters as in Fig. 3, except that $k=3.0$.

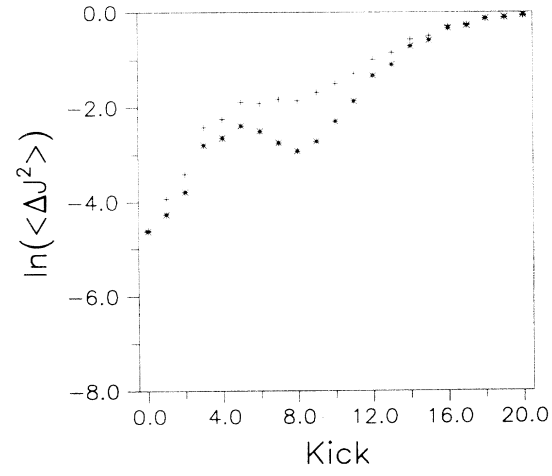

FIG. 8. The same quantities and parameters as in Fig. 7, but with a uniform circular disk satisfying Eq. (57) for the initial classical ensemble.

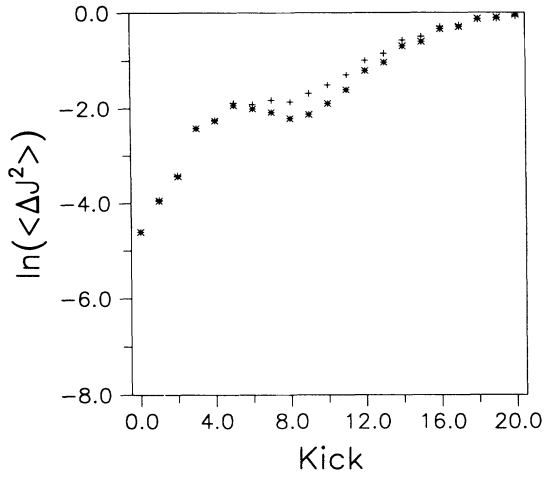

FIG. 9. The same quantities and parameters as in Fig. 8, but with a uniform elliptical disk satisfying Eq. (57) for the initial classical ensemble.

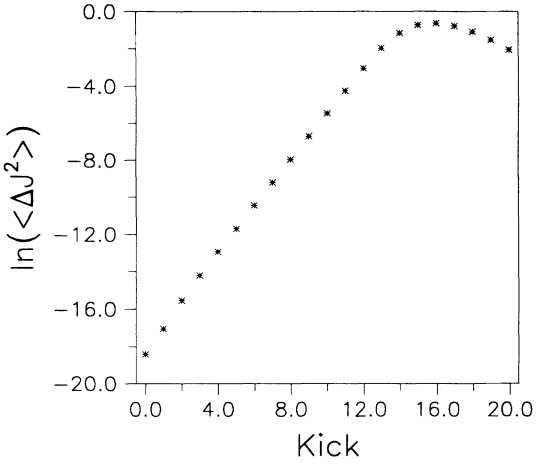

FIG. 11. The same classical quantities and parameters as in Fig. 1, except that $j=10^8$.

missing from the numerical work of Nakamura and co-workers [10] because their parameter values are such that the local expansion rate is so large, and for it the initial distribution is broad enough ($j=128$) that saturation occurs just after the first kick. By the second kick their distribution supersaturates and has wrapped itself around the ϕ domain about five times.

Since the initial uncertainty product for the angles is of order $1/j$, the number of kicks, n, required to achieve saturation when the local, transient expansion rate is λ must be given by

$$\exp(n\lambda)\approx j \ . \tag{58}$$

This is similar to the relation published by Haake, Kus, and Scharf [11] (in [11], λ denotes the global Lyapunov exponent). For Fig. 1 we find $\lambda=1.2$ for the first four kicks, which is consistent with Eq. (58) since full saturation does not occur until kick 6. In the calculations by Nakamura and co-workers [10], $j=128$ and $\lambda\approx 40$, which imply $n \ll 1$ according to Eq. (58). The rapid oversaturation seen from kick 1 to kick 2 in their results is a consequence of the highly chaotic behavior of the top that is associated with their choice of parameters (it often happens that very little change is seen between the initial state and kick 1 [4]).

Instead of using the highly accurate Gaussian distribution given by Eq. (53) for the initial classical ensemble, Haake, Kus, and Scharf, [11] used a uniform circular disk matching the size of the uncertainty, $\Delta\Omega=1/j$, for the generalized coherent state. Figure 2 shows the results for the same parameter values used for Fig. 1. The quantum plus signs are the same as in Fig. 1 but the classical asterisks obtained for a uniform disk (with radius $2/\sqrt{j}$ [11]) are not nearly so good. However, if we use this uniform disk to compute the left-hand side of Eq. (57), we find $2/j$

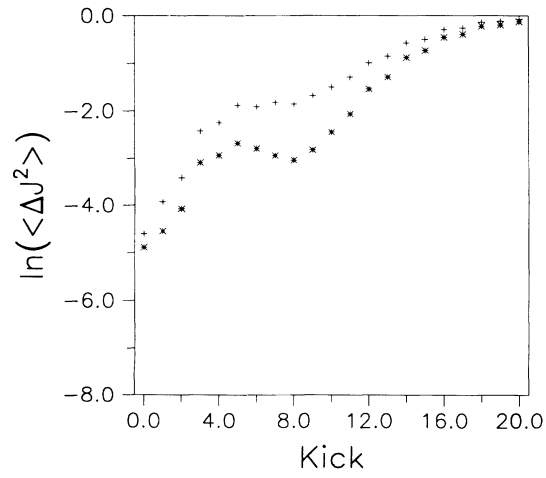

FIG. 10. The same quantities and parameters as in Fig. 7, but with a Gaussian distribution that does not include the $\sin^2(\theta)$ term in Eq. (53) for the initial classical ensemble.

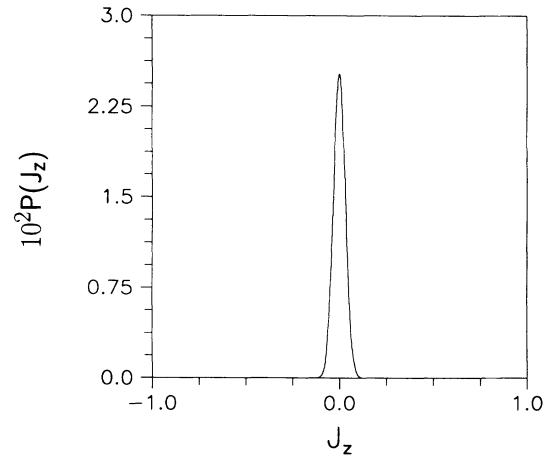

FIG. 12. Absolute probability distribution for J_z for the parameters used in Fig. 1. This is the initial distribution quantum mechanically. The abscissa is divided into 1001 m values.

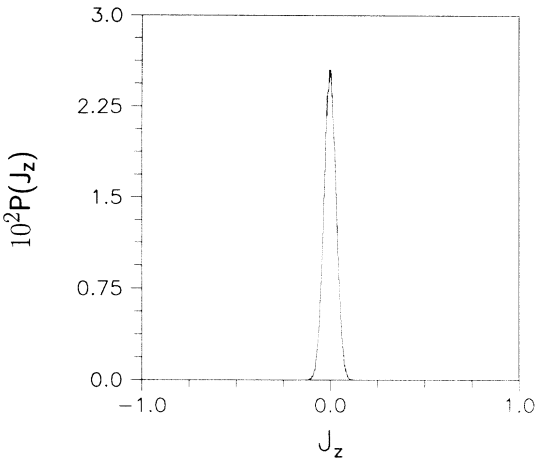

FIG. 13. Classical version of Fig. 12 for an ensemble of 50 000 points.

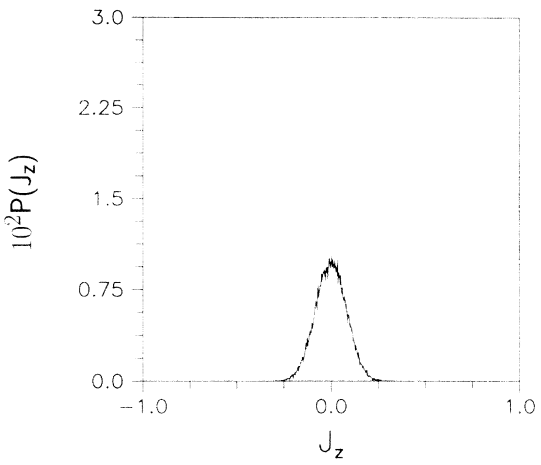

FIG. 15. Same as Fig. 13 for kick 2.

instead of $1/j$. We can adjust the radius of the circular disk (use $\sqrt{2}/\sqrt{j}$ instead) in order to make the result agree with $1/j$. When this is done, we obtain Fig. 3. The agreement between the quantum and classical results is better than in Fig. 2 but still inferior to Fig. 1. Differences are already discernible by kick 4 in Fig. 3, while they begin with the initial states in Fig. 2 because the left-hand side of Eq. (57) is not $1/j$ for Fig. 2.

Figures 4, 5, and 6 reiterate these results for the same parameter values except that **k** is increased to 3.0, which makes the dynamics more chaotic. Figure 4 shows excellent quantum-classical correspondence for 20 kicks with an exponential stage of three kicks, saturation at four kicks, and discernible differences beginning at kick 8 or 9. Figure 5 for the uniform classical disk, but not satisfying: the left-hand side of Eq. (57) equals $1/j$, and shows a lack of correspondence from the start, while Fig. 6 shows better correspondence, because the left-hand side of Eq. (57) equal to $1/j$ is imposed on the disk size, with small differences arising at kick 4.

In each of the preceding cases, the generalized coherent state parameter θ was taken to be $\pi/2$. This means that the $\sin^2(\theta)$ in the ϕ distribution of Eq. (53) is simply 1. This is the reason that the initial classical ensemble may be approximated as a circle as has been done by Nakamura and co-workers [10] and Haake, Kus, and Scharf [11]. One motivation for this choice is to choose a region of phase space well outside the islands of regular motion. However, if θ is taken to be $\pi/4$, say, then the Gaussian distribution in Eq. (53) no longer has a circular cross section (it is now an ellipse), and one is still outside the islands of regular motion. We believe this observation previously has been missed. Figure 7 shows that our Gaussian distribution continues to work extremely well for this case too. Figure 8 shows that a uniform circular disk with the left-hand side of Eq. (57) equal to $1/j$ imposed works less well, and Fig. 9 shows that a uniform elliptical disk is much better than Fig. 8, but still not as good as Fig. 7. Figure 10 shows what happens if you use our Gaussian distribution but leave out the $\sin^2(\theta)$ factor. In this example, we have also taken $\phi=\pi/4$ and $k=1.865$. There is an interesting anomaly at the third

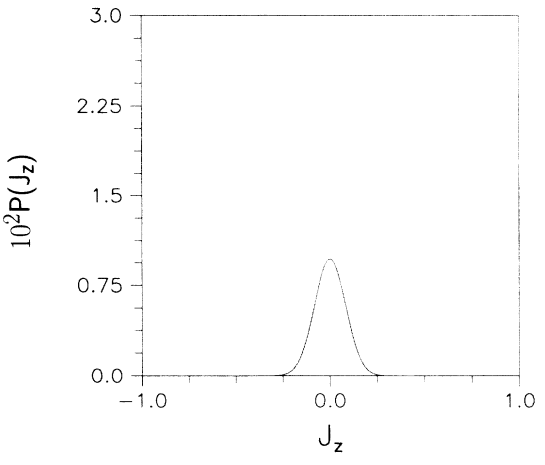

FIG. 14. Same as Fig. 12 for kick 2.

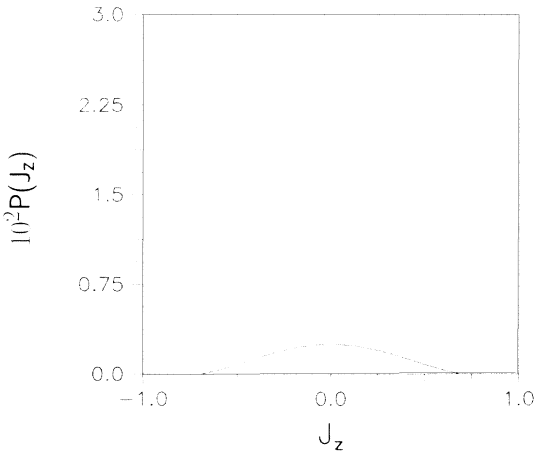

FIG. 16. Same as Fig. 12 for kick 4.

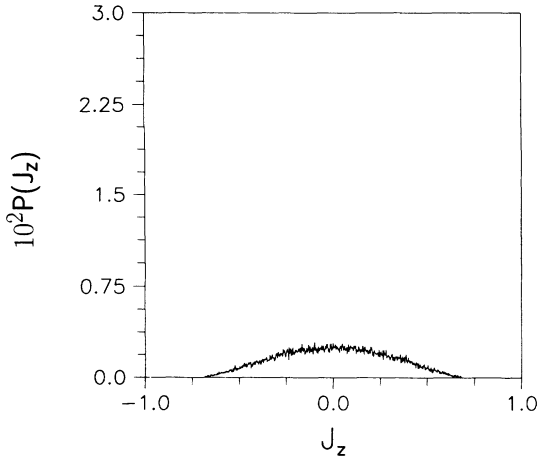

FIG. 17. Same as Fig. 13 for kick 4.

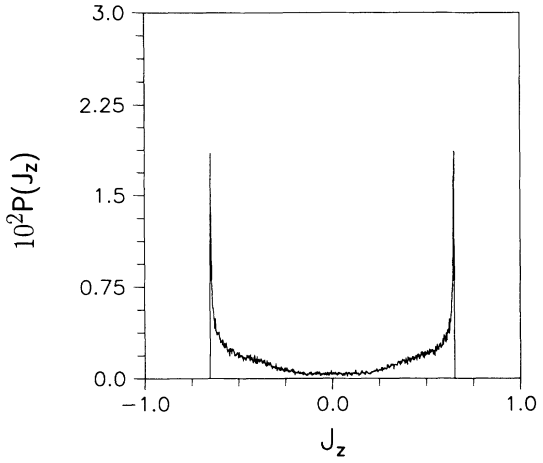

FIG. 19. Same as Fig. 13 for kick 7.

kick in Fig. 7. If it were not there, the first four kicks would exhibit a nearly perfect exponential growth stage satisfying the saturation condition Eq. (58). What is happening can be seen by looking at a plot of the classical distributions as they evolve. With each kick the distribution grows and shifts its location in phase space by jumps. In this case, by chance, the distribution after the third kick is almost exactly half on the positive J_y side and half on the negative J_y side of the phase space. Thus the mean J_y value is anomalously small for the third kick and this creates the anomalous enhancement of the total variance. The quantum distributions behave the same way.

When the initial wave packet and the corresponding initial ensemble are sufficiently sharply peaked, there is always very good quantitative agreement between the quantum and classical growth of the variances. By making the initial variances as small as possible, it is possible to increase the number of kicks that occur during the initial exponential growth stage [4]. To do this for the classical ensemble requires no special numerical techniques, but to do it for the quantum wave packet is prohibitive for large j. Already for j of the order of 10^4, the computation of the Jacobi polynomials overwhelms our computer. Since we know [9] both the quantum and classical behaviors are initially the same, we can perform a classical calculation for large j to represent the quantum-classical correspondence. In Fig. 11 we show the results for the parameters used in Fig. 1 but with $j=10^8$. Now we see 14 kicks during the exponential stage, as is consistent with the expectations implied by Eq. (58).

It is instructive to view the evolving shapes of the quantum and classical distributions. In Figs. 12–23, we show the J_z distributions for the case of Fig. 1. Figures 12 and 13 show the quantum and classical initial distributions respectively. Since $j=500$, each J_z axis is divided into 1001 bins (for $2j+1$ m states) and the absolute probabilities are shown. Figures 14 and 15 show kick 2. Figures 16 and 17 show kick 4. Figures 18 and 19 show kick 7. Since kick 7 is well past saturation, in Fig. 18 we see the quantum interference effects that began with kick 5 and which are impossible for the classical distribution. Figures 20 and 21 show kick 15. One sees a partial re-

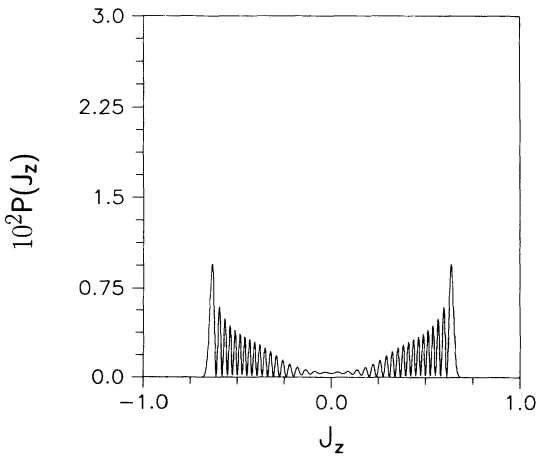

FIG. 18. Same as Fig. 12 for kick 7.

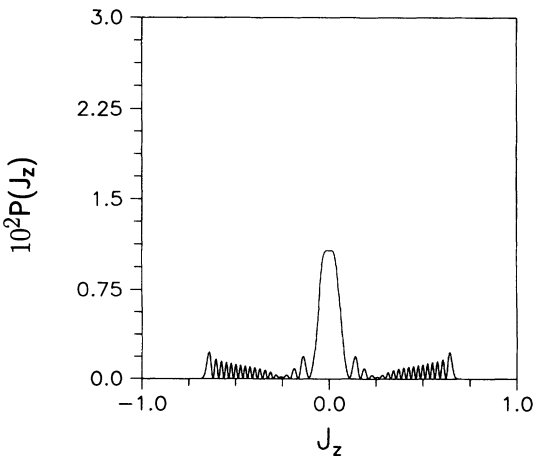

FIG. 20. Same as Fig. 12 for kick 15.

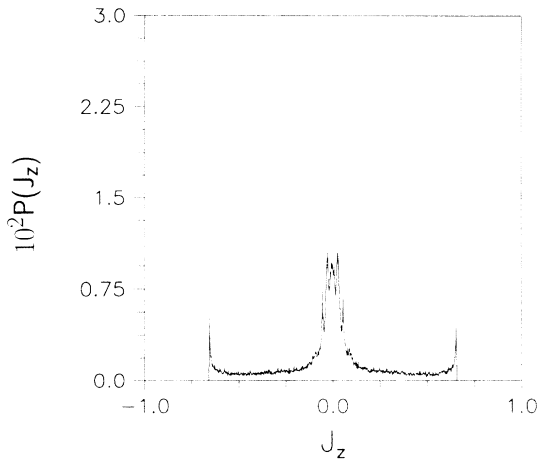

FIG. 21. Same as Fig. 13 for kick 15.

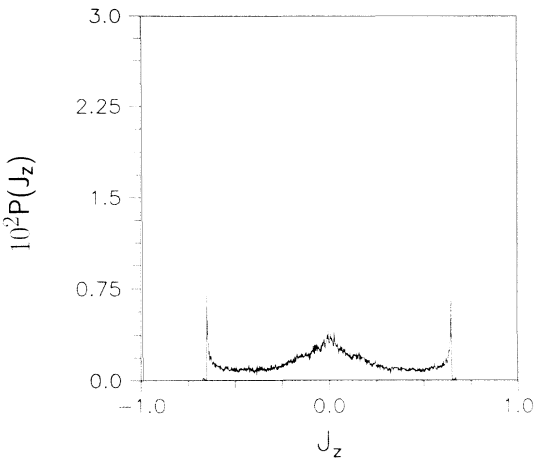

FIG. 23. Same as Fig. 13 for kick 20.

currence of the initial distribution which reflects the damped oscillation seen in Fig. 1, and similarly seen more dramatically for more chaotic parameter values in Fig. 4. Figures 22 and 23 show kick 20. Thus the strong quantitative quantum-classical correspondence seen during the exponential growth stage is followed by different behavior after saturation. Nevertheless, by coarse graining the quantum interference patterns, one obtains a distribution very similar to the classical distribution. For kick 7, coarse graining makes the quantum distribution virtually identical with the classical, but for kicks 15 and 20, even after coarse graining, there remain differences in the region of the abscissa between ± 0.1 and ± 0.25.

IV. CONCLUDING REMARKS

The results presented in this paper for the kicked top extend our earlier work on chaos and quantum-classical correspondence [4,5,9]. The classical concepts of phase space and Lyapunov exponents are captured quantum mechanically by smoothed Wigner distributions and the initial, exponential rate of growth of quantum variances.

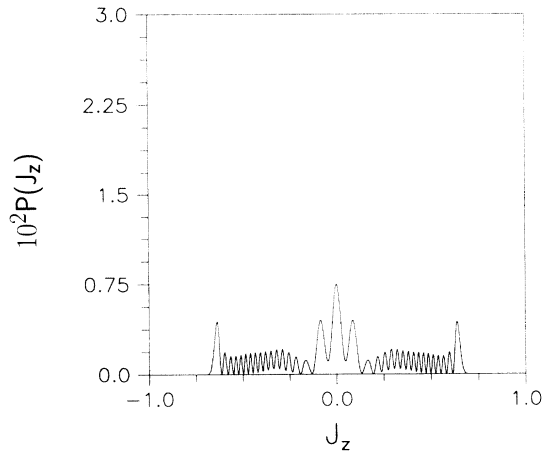

FIG. 22. Same as Fig. 12 for kick 20.

Originally [9], it was shown that the classical Jacobi matrix provides the link between classical chaos and the rate of growth of quantum variances. This realization grew out of studies concerned with the growth of intrinsic fluctuations in classical macroscopic systems [17–20]. Consequently, we approached the chaos and quantum-classical correspondence problem from a general perspective rather than from the behavior of some particular model system, such as the kicked pendulum, the cat map, or the kicked top. This explains why we have been able to obtain results for these particular models that had not been seen previously.

Smoothing of the Wigner distribution creates the Husimi-O'Connell-Wigner distribution which is a true probability distribution. For the kicked pendulum, we used harmonic oscillator coherent states [4], as was suggested by earlier work by Chang and Shi [7]. In fact, we simply evolved Gaussian wave packets that were constructed to be equivalent with the Husimi-O'Connell-Wigner distributions created by smoothing with an ordinary coherent state. For the cat map [5], we simply used a Gaussian wave packet directly. However, one could view the wave packet as equivalent to a corresponding smoothed Wigner distribution. For the kicked top presented here, we used generalized coherent state smoothing of a generalized coherent state, which is again equivalent to smoothing a Wigner distribution and leads to a Gaussian wave packet. The generality of this approach is manifest.

What we see in each case is that for a sufficiently sharply peaked initial wave packet there corresponds a classical ensemble, and for both the evolution of corresponding variances is initially exponential. The exponential rate of growth is the local, transient, classical expansion rate, that is determined by the evolving Jacobi matrix. Normally, this property is not a uniform property of phase space and as a consequence the local expansion rate is not identical with the global Lyapunov exponent. However, for the cat map the expansion rate is uniform and we showed [5] that a quantum measurement actually yields the largest classical Lyapunov exponent with great

accuracy in that case.

In this paper, we have presented a properly normalized Gaussian ensemble correspondent for a SU(2) generalized coherent state. This provides a quantitative improvement over previously published uniform ensembles that merely approximate the Gaussian ensemble. Even for finite values of j, for which the quantum Hilbert space is finite, the generalized coherent states behave just like the corresponding classical ensembles during the initial exponential growth stage of the variances, provided the initial state is sufficiently sharply peaked. Thus quantum-classical correspondence for a chaotic classical dynamics does not require notions involving infinite time, and the quantum description is actually only quasiperiodic. This underscores the advantage of viewing chaos and quantum-classical correspondence from the perspective of quantum wave packets and associated classical ensembles.

ACKNOWLEDGMENTS

This work was supported by National Science Foundation Grant No. 92-03878. We thank Boris Chirikov for bringing the work of Nakamura and co-workers to our attention.

[1] B. V. Chirikov (unpublished).
[2] F. Haake, *Quantum Signatures of Chaos* (Springer-Verlag, Berlin, 1991).
[3] E. Heller and S. Tomsovic, Phys. Today **46** (7), 38 (1993), and references therein.
[4] R. F. Fox and T C. Elston, Phys. Rev. E **49**, 3683 (1994).
[5] T. C. Elston and R. F. Fox (unpublished).
[6] T. Dittrich and R. Graham, in *Instabilities and Nonequilibrium Structures II,* edited by E. Tirapegui and D. Villarroel (Kluwer Academic, Dordrecht, 1989); Ann. Phys. **200**, 363 (1990).
[7] S.-J. Chang and K.-J. Shi, Phys. Rev. A **34**, 7 (1986).
[8] R. F. O'Connell and E. P. Wigner, Phys. Lett. **85A**, 121 (1981).
[9] R. F. Fox, Phys. Rev. A **41**, 2969 (1990).
[10] K. Nakamura, A. R. Bishop, and A. Shudo, Phys. Rev. B **39**, 12 422 (1989); K. Nakamura, Y. Okazaki, and A. R. Bishop, Phys. Rev. Lett. **57**, 5 (1986).
[11] F. Haake, M. Kus, and R. Scharf, Z. Phys. B **65**, 381 (1987).
[12] W.-M. Zhang, D. H. Feng, and R. Gilmore, Rev. Mod. Phys. **62**, 867 (1990).
[13] J. J. Sakurai, *Modern Quantum Mechanics* (Benjamin/Cummings, Menlo Park, CA, 1985), Chap 3.
[14] R. J. Glauber, in *Fundamental Problems in Statistical Mechanics II,* edited by E. G. D. Cohen (North-Holland, Amsterdam, 1968).
[15] A. R. Edmonds, *Angular Momentum in Quantum Mechanics,* 2nd ed. (Princeton University Press, Princeton, 1960), p. 58.
[16] D. E. Knuth, *The Art of Computer Programming* (Addison-Wesley, Reading, MA, 1969), Vol. 2
[17] R. F. Fox and J. E. Keizer, Phys Rev. Lett. **64**, 249 (1990).
[18] J. Keizer, R. F. Fox, and J. Wagner, Phys. Lett. A **175**, 17 (1993).
[19] R. F. Fox and T. C. Elston, Chaos **3**, 313 (1993).
[20] T. C. Elston and R. F. Fox, Chaos **4**, 1 (1994).